

Published in final edited form as:

*Biomaterials*. 2013 January ; 34(2): 353–360. doi:10.1016/j.biomaterials.2012.09.071.

## Directing cell migration in continuous microchannels by topographical amplification of natural directional persistence

Young-Gwang Ko, Carlos C. Co, and Chia-Chi Ho\*

Department of Chemical and Materials Engineering, University of Cincinnati, Cincinnati, OH 45220, USA

### Abstract

Discrete micropatterns on biomaterial surfaces can be used to guide the direction of mammalian cell movement by orienting cell morphology. However, guiding cell assembly in three-dimensional scaffolds remains a challenge. Here we demonstrate that the random motions of motile cells can be rectified within continuous microchannels without chemotactic gradients or fluid flow. Our results show that uniform width microchannels with an overhanging zigzag design can induce polarization of NIH3T3 fibroblasts and human umbilical vein endothelial cells by expanding the cell front at each turn. These continuous zigzag microchannels can guide the direction of cell movement even for cells with altered intracellular signals that promote random movement. This approach for directing cell migration within microchannels has important potential implications in the design of scaffolds for tissue engineering.

### Keywords

Cell migration; Microchannel; Gelatin; Directional movement

### 1. Introduction

Significant advances have been made in the three-dimensional fabrication of biodegradable scaffolds [1–4]. With recent developments in two photon polymerization, scaffolds may be fabricated with sub-micron resolution [5–8]. However, the assembly of functional tissue composed of precisely assembled structures of different cell types remains a challenge. The limited tolerance of mammalian cells to shear, in particular, constrains the high speed manipulation and seeding of individual cells. Thus, while scaffolds can be fabricated with sub-micron resolution, on a practical scale different cell types may only be seeded as large clumps. Directing cells to migrate from these reservoirs to specific positions within the scaffold is a fundamental problem because cells move bidirectionally in microchannels resulting in no net displacement [9–11]. Modulating the channel width akin to a series of “fish traps” may be used to direct cell migration [12], but the constrictions lead to stuck cells and severely retards migration. Here, we present a new approach for topographically amplifying the natural directional persistence (TANDIP) of cells to direct their migration along continuous microchannels of uniform width with minimal hindrance.

© 2012 Elsevier Ltd. All rights reserved.

\*Corresponding author. Tel.: +1 513 556 2438; fax: +1 513 556 3473 hocc@ucmail.uc.edu. .

**Appendix A. Supplementary data** Supplementary data related to this article can be found at <http://dx.doi.org/10.1016/j.biomaterials.2012.09.071>.

Research on directional migration has focused extensively on cellular response to gradients of chemoattractants, extracellular matrix (ECM), substrate stiffness, and shear flow that induce chemotaxis, haptotaxis, durotaxis, and mechanotaxis respectively [13–15]. However, the limited window of external gradients that cells are compatible with and respond to restricts the range of directional guidance. To overcome this, we and others have engineered biomaterials with surface micropatterns that amplify the natural directional persistence (MANDIP) of cells [16–18]. Relying solely on asymmetric microarrays of cell-adhesive islands, MAN-DIP is a gradient-free approach that enables simultaneous control on the direction and speed of migration of unlimited number of cells over unlimited distances on preset paths of arbitrary complexity. MANDIP's dependence on arrays of cell-adhesive islands to intermittently constrain cell shape and directionally rectify "hopping" motions, however, precludes its extension to three dimensions as the islands do not present a continuous path for cells to migrate. The ability to guide the organization and composition of different cell types by directing their migration from reservoirs along three-dimensional biodegradable microchannels would be invaluable for creating complex regenerative tissue architectures.

## 2. Materials and methods

### 2.1. Materials

Polydimethylsiloxane (PDMS, Sylgard 184 silicone elastomer base and curing agent) was purchased from Dow Corning. Gelatin (porcine skin, Type A, G2500) was obtained from Sigma Aldrich. Poly(oligo(ethyleneglycol) methacrylate-*co*-methacrylic acid) (poly(OEGMA-MA)) was prepared by free radical polymerization of methoxy poly(ethylene glycol) monomethacrylate (OEGMA: 80 wt%, 550Da oligo(ethyleneglycol) units, Scientific Polymer Products Inc.) and methacrylic acid (MA: 20 wt%, Scientific Polymer Products Inc.) and 0.1 wt% fluorescein-*O*-methacrylate (Sigma Aldrich Inc.) with 0.1 wt% 2,2'-azobis (2-amidinopropane) dihydrochloride (Wako Pure Chemical Industries, Ltd.) as an initiator for 24 h at 60 °C [19]. Phalloidin (Alexa Fluor 488 phalloidin), DAPI (4',6-diamidino-2-phenylindole) and BODIPY TR ceramide (N-((4-(4,4-difluoro-5-(2-thienyl)-4-bora-3a, 4a-diaza-s-indacene-3-yl)phenoxy)acetyl)sphingosine) were obtained from Molecular Probes.

### 2.2. Fabrication of microchannels on gelatin substrates

The patterns were printed on a chrome mask and silicon masters were fabricated by photolithography. The silicon master was coated with (tridecafluoro-1,1,2,2-tetrahydro-octyl)-1-trichlorosilane (United Chemical Technologies, Inc.) by vacuum evaporation before pouring polydimethylsiloxane (PDMS) prepolymer (mixed in 10.0 wt% curing agent) to mold the pattern on the PDMS stamp. After curing at 60 °C for 2 h, the PDMS stamp was detached from the silicon master, rinsed with 70% ethanol then applied to mold the three-dimensional microchannel on the gelatin film. The channel patterns on the PDMS stamp were transferred to a gelatin substrate by cryogenic indentation. Gelatin solution (15.0 w/w %) was prepared by dissolving gelatin powder in deionized water at 60 °C. Warm gelatin solution was spread on a glass slide and the PDMS stamp was applied to mold the gelatin. The PDMS stamp-gelatin construct was kept on a cold iron plate (−20 °C) for 15 s before peeling the PDMS stamp away. The gelatin film was returned to room temperature, crosslinked with glutaraldehyde (1.0 w/w%) for 2 h, immersed in glycine (50 mM) overnight, and dried at room temperature. The dimensions of the microchannels were measured by KLA-Tencor P15 Profilometer and Nikon TE2000 inverted microscope. To prevent cell attachment outside the microchannels, a flat PDMS stamp with cell resistant poly(OEGMA-MA) was printed to the plateau regions of the gelatin film then maintained at 60 °C for a week.

### 2.3. Cell culture

NIH3T3 fibroblasts and their mutants with constitutively activated Rac1, RhoA, and Cdc42 (Rac1L61, RhoA63 and Cdc42L61) were gifts from Y. Zheng (Cincinnati Children's Hospital). The mutants were prepared by site-directed mutagenesis based on oligonucleotide mediated PCR [20]. Primary human umbilical vein endothelial cells (HUVEC) were purchased from American Type Culture Collection. Gelatin films (25 × 30 mm) were incubated with 1.0 v/v% Penicillin-Streptomycin-Neomycin Antibiotic Mixture (PSN, GIBCO, Invitrogen) for 30 min, rinsed with phosphate buffered saline (PBS) solution and the cell media. Iscove's Modified Dulbecco's Medium (IMDM, GIBCO, Invitrogen) supplemented with fetal bovine serum (10.0 v/v %, FBS) and PSN (1.0 v/v%) was used as the cell media for fibroblasts and Endothelial Cell Basal Medium-2 (EBM-2, Lonza) supplemented with endothelial cell growth kit for HUVEC. Cells were plated on the gelatin substrate (500 cells/cm<sup>2</sup>) with medium containing FBS (10.0 v/v%) and incubated under 5% CO<sub>2</sub> at 37 °C. The culture media was refreshed to a mixture of Opti-MEM and IMDM (80:20 v/v%) with PDGF (5 ng/mL) for fibroblasts and Opti-MEM and EBM-2 (80:20 v/v %) supplemented with rhEGF (10 ng/mL) for HUVEC 1 h prior to tracking to promote cell migration [21].

### 2.4. Fluorescence microscopy

Staining of cells for actin, nuclei, and Golgi apparatus followed standard protocols. Cells were washed with PBS and fixed with 3.7% methanol free formaldehyde for 10 min, and permeabilized with 0.2% Triton X-100 for 5 min. After rinsing with PBS the cells were incubated with phalloidin and DAPI to stain F-actin and nucleus for 40 min. Golgi apparatus was stained with BODIPY TR ceramide. Images of the stained cells were collected using a Nikon TE2000 inverted microscope equipped with a SPOT Diagnostic CCD camera and analyzed with Metamorph software (Universal Imaging).

### 2.5. Imaging and statistical analysis

Time-lapse phase contrast images were collected using a Nikon TE2000 inverted microscope under a phase contrast mode. Cells were tracked 8 h after seeding for 24 h at 6 h intervals. Directionality and movement frequency were measured from sequential photomicrographs based on the location of the cell nucleus. Only cells that did not divide or form contacts with other cells within the 24 h period were analyzed. A minimum of 50 separate cells were analyzed for each pattern. Statistical analysis was examined by the mean and the standard deviation using data analysis software (KyPlot version 2.0, KyensLab, Inc.). Significance levels were determined by one-way ANOVA (analysis of variance) with a parametric multiple comparison of post-hoc test by Tukey's method. Statistical significance was considered as  $p < 0.05$ .

## 3. Results and discussion

On two-dimensional surface micropatterns composed of four connected cell-adhesive rectangles, cells move clockwise and counterclockwise with equal probability (Fig. 1A). When the cyclic path of four connected rectangles is nicked with 5.4 μm gaps, cells are intermittently constrained, and the asymmetric arrangement of the islands result in a significant directional bias (Supplementary Fig. 1). Individual NIH3T3 fibroblasts intermittently constrained within the adhesive rectangles extend lamellipodia from both ends along envelopes preferentially aligned to their elongated bodies. On one end, extended lamellipodia can span the 5.4 μm gap and attach to an adjacent island. On the other end, island hopping would require aberrant extension and attachment of lamellipodia 90° relative to the long axis of the cell body. This MANDIP approach is very effective on two-

dimensional surfaces, but the gaps necessary to confine cells intermittently, preclude its direct extension to continuous three-dimensional microchannels.

### 3.1. Directing cell migration with microchannels on biomaterials

Inspired by the observation that cells with elongated morphology initiate movement only from their ends and not from their midsection, we eliminated the gaps and offset the cyclic pattern to form overhangs at each corner. With no gaps, this pattern can be fabricated as a three-dimensional cyclic microchannel (Fig. 1B) where the dimensions of the rectangular wells on each side are chosen to accommodate individual cells snugly [11,16,17]. In this manner, we hypothesized that one end of the cells will be trapped in the overhanging section and migration in the reverse direction would be suppressed. Using soft lithography and cryoindentation, we fabricated topographical microchannels of this design on gelatin. The average depth of channels was 1.5  $\mu\text{m}$  (Supplementary Fig. 2). The plateau regions outside the microchannels were stamped with poly(oligo(ethyleneglycol) methacrylate-*co*-methacrylic acid) (poly(OEGMA-MA)) to limit seeding of cells exclusively within the microchannels [19] (Fig. 2). With the proper choice of channel dimensions, significant directional bias can be achieved in cyclic overhang microchannels (Fig. 1C, Table 1). Cells migrate continuously within the microchannels with 79% of turns in the clockwise direction and 21% of turns in the counterclockwise direction. Cells on the same continuous cyclic overhang micropatterns on 2D surfaces also exhibit preferential movement in the clockwise direction. Although cells on 2D micropatterns do bridge the interior cell resistant background at the 90° turns, which does not occur for cells within the 3D microchannels. Control experiments along microchannels without overhanging structures on 2D micropatterns or 3D microchannels show no observable directional preference in either direction (data not shown).

The cyclic microchannel guides directional cell movement effectively, but the net translocation is limited. Rearranging the rectangular segments, as shown in Fig. 3A, enables cells to move large distances within one-way microchannels. For this zigzag microchannel geometry with 90° angles between segments, 78% of observed fibroblast movements were to the right (Table 1). Human umbilical vein endothelial cells (HUVEC) also migrate directionally (Fig. 3B) but with a reduced bias of 59%. HUVEC extends broader, but shorter lamellipodia compared to fibroblasts, and this difference likely affects the efficacy of the overhangs in rectifying cell migration.

### 3.2. Effects of interconnection angle

In addition to providing directional guidance, the flux of the cellular traffic can be modulated by the angle at the T-junctions. Compared to microchannels with 90° turns, NIH3T3 fibroblasts and HUVECs show a decrease in the rate of segment traversal on sharper 60° turns and an increase on gradual 120° turns (Fig. 3 and Table 1). The distribution of migration events and frequencies for the different pattern designs are shown in Supplementary Fig. 3. Patterns with sharper or more gradual turns both direct the movement of fibroblasts with minimal changes to the directional bias, while endothelial cells increase their directional bias in microchannels with more gradual turn angles at 120°. The angle between the segments influence the bending necessary for the cell to traverse the turns, which is related to cell contractility that differs between cell types [22]. The net horizontal velocity (Table 1), which is the combined result of the horizontal displacement per segment, directional bias, and segment traversal rate, is in all cases maximized on the patterns with gradual 120° turns. Although the speed of individual cell movements in microchannels is slower compared to cells on flat substrates [23,24], random cell movements lead to negligible net translocation compared to the horizontal velocities (100–400  $\mu\text{m}/\text{day}$ ) observed here. Using high resolution 3D printers, TANDIP patterns may be

printed between clumps of different cell types spaced, e.g., ~1 mm apart, from which the cells propel themselves to their final destinations within the printed tissue over 3–10 days. This overcomes the challenge of robotically positioning individual cells whose shear sensitivity limits the rate at which they may be manipulated.

### 3.3. The mechanisms of directed cell movement on the microchannels

A complementary mechanism for the observed directional migration is the polarity induced by the expanding cell shape as cells traverse the overhanging zigzag patterns. Free cells adopting teardrop shapes migrate with a modicum of natural directional persistence because of preferential migration from their broad leading edge relative to movements initiated from their midsection or from their narrow rear. Fig. 3C shows that NIH3T3 fibroblasts confined along the rectangular segments adopt elongated shapes and align their actin filaments along their extended body. Upon approaching a T-junction, extended lamellipodia spread to occupy both arms of the T-junction leading to a polarized morphology with a wide leading edge and a narrower tail. The protrusion ceases at the dead end but continues in the other direction. This process repeats itself with the T-junctions reconfiguring the cells to adopt a Y-shape morphology and with the dead ends, cells are forced to make alternating turns resulting in net displacement towards the right. Lamellipodia extended toward the overhanging dead ends are observed, but are narrower and less pronounced than in the direction toward the T-junctions. For cells that do not have one end already trapped in the dead end segment, and moving leftwards, they have a choice of entering the dead end segment or making a turn to continue their leftwards migration. In this case, the envelope of lamellipodia extension is aligned with the elongated cell body as observed in MANDIP [16–18], and the cells are more likely to migrate into the dead end segment. These observations suggest that although the channels have a constant width, a migrating cell senses an expansion at each T-junction, which leads the cell forward by defining its polarity. Golgi apparatus are localized in front of the nuclei in migrating cells [25,26]. Visualizing the distribution of Golgi apparatus relative to the nuclei within fibroblasts traversing the overhanging zigzag patterns (Fig. 3D) confirm that the T-junctions indeed direct cell movement by inducing morphological polarization. The overhanging zigzag patterns topographically amplify natural directional persistence (TANDIP) by (1) intermittently defining a cell end and cell midsection from which migration is suppressed, and (2) intermittently offering opportunities to form broad polarizing edges at the T-junctions to lead cells out of the rectangular segments.

### 3.4. Effects of GTPases activation on cell movement

Previous studies on bare tissue culture substrates have shown that global activation of intracellular signals that mediate lamellipodia extensions (Rac1) and regulate cell polarity (Cdc42) reduce the natural directional persistence of fibroblast migration and promote random migration [27]. To test the robustness of TANDIP in guiding directional movement, we investigated the migration of cells expressing constitutively activated Rac1 or Cdc42. Remarkably, activating the intracellular signaling pathways promoting random migration causes only a slight reduction of directional bias and increases the speed of cell movement on all patterns with different angles (Figs. 4 and 5 and Table 1). Cells expressing constitutively activated Rac1 migrate at a faster speed consistent with the increased formation of peripheral lamellae [28]. The minor reduction in directional bias of cells with constitutively activated Rac1 demonstrates that TANDIP microchannels are capable of providing directional guidance even for cells with intracellular signaling that disrupt directional movement. Cells with constitutively activated Cdc42 that lead to random movement on non-patterned substrates exhibited directional movement with 63% bias for different junction angles. The larger reduction of directional bias for cells expressing constitutively activated Cdc42 compared to Rac1 point to the more significant role of Cdc42



in establishing cell polarity. Cdc42 activation also increases the speed of cell movement and consistent with the tendency of Cdc42 to increase actin polymerization and protrusion of filopodia [27].

When fibroblasts move along the microchannels their rear attachments do not release immediately and sometimes leave long tails as cells move onwards to the next segment (Fig. 3A). Slow retraction suggests that accelerating rear adhesion disassembly by intracellular signals such as RhoA can increase cell velocity. We confirmed this by quantifying the rate of movement of NIH3T3 fibroblasts expressing constitutively activated RhoA. As expected, RhoA activated cells exhibit reduced tail length and moved at nearly double the velocity of the wild type (Fig. 4). The directional bias for RhoA activated cells is similar to wild type fibroblasts on 120° microchannels and reduced slightly on 60° and 90° microchannels. These results demonstrate that one-way TANDIP microchannels can impose directional bias while intracellular signals such as activation of Rac1, Cdc42, and RhoA can tune the speed and tendency of cells to move in the preset direction.

It is interesting to note that cells do not move at a steady pace through the microchannels. Fig. 6 superimposes the centroids of cell nuclei from over 50 time-lapse images for each pattern design. Each rectangular segment was divided into four sections of equal area (overhang, T-center, middle, T-entry). If the centroids move at a constant rate, then the centroids would be uniformly distributed among the sections. Instead, only ~6% of the centroids were located in the overhangs, ~18% in the middle sections, ~34% for the entry region of the T-junctions, and ~42% for the center region of the T-junctions. This indicates that cells decelerate to make the turn at each T-junction.

The TANDIP design principles described here for directing cell migration with tunable velocities can be implemented on biomaterials with one-way microchannels oriented and interconnected in all three dimensions using a range of printing, deposition, and optical techniques [2,5,8]. With further refinement, three-dimensional printers may be able to routinely form biodegradable sub-micron features, but would still be limited to printing >200  $\mu\text{m}$  clumps (reservoirs) of cells from separate lower resolution nozzles to avoid subjecting cells to high shear stresses. From these reservoirs, printed TANDIP microchannels can guide the simultaneous migration of unlimited number of cells to their final destinations individually. By relying on self-propelled cellular migration and minimizing the need for robotic positioning of cells, TANDIP can be eminently useful in the bottom-up assembly of complex regenerative tissues with single cell resolution.

## 4. Conclusions

We have demonstrated the design principle and fabrication of TANDIP microchannels capable of guiding self-sustained directional cell movement without external gradient or shear stress. The topography of the channels promotes cell movement through the main channel in the direction opposite to the dead end overhanging segments. Each T junction amplifies the directional persistence forwards by promoting polarized morphology at the junction and suppressing backward movements that would require the unfavorable protrusion of lamellipodia from midsection of the elongated cells. The pattern design and intracellular signals on contractility can tune the flux of cellular traffic. Some of the differences in the directional bias as a function of segment angle can be attributed to differences in the cytoskeletal structure evident in the shape of the cells on flat substrates (fan shaped for the HUVECs and more elongated spindle shape for fibroblasts). However, details of how different cells sense and respond to the topography of different microchannel designs remain unclear.

Remarkably, the TANDIP microchannels can also guide cells that otherwise exhibit random movement on substrates such as CA-Rac1 and CA-Cdc42 cells. The design principle can be applied directly on biomaterials with microchannels oriented and interconnected in all three dimensions using three-dimensional inkjet printing processes or photodegradable hydrogels. With further refinement, inkjet printers may ultimately be able to print biodegradable features smaller than 10  $\mu\text{m}$ , but would still be limited to printing  $>100 \mu\text{m}$  clumps (reservoirs) of cells from separate lower resolution nozzles to avoid subjecting cells to high shear stresses. TANDIP microchannel designs can be eminently useful in guiding cells from these reservoirs precisely to their final destinations and has promise in scaffolds designs in which cell movement are simultaneously and individually directed in real time to interact with the 3D microenvironments. TANDIP guided motion of mammalian cells has promising applications in temporal and spatial regulation of cellular assemblies in 3D biomaterials for tissue regeneration and for directing cells in lab on a chip devices.

## Supplementary Material

Refer to Web version on PubMed Central for supplementary material.

## Acknowledgments

This research was supported by the National Institutes of Health (R01EB010043) and the National Science Foundation (CBET0928219). We thank Ross Andrews for synthesizing the cell resistant poly(OEGMA-MA), Dr. Girish Kumar for helpful discussions, and Rebecca Moore for performing some preliminary studies.

## References

- [1]. Hahn MS, Miller JS, West JL. Three-dimensional biochemical and biomechanical patterning of hydrogels for guiding cell behavior. *Adv Mater.* 2006; 18:2679–84.
- [2]. Kloxin AM, Kasko AM, Salinas CN, Anseth KS. Photodegradable hydrogels for dynamic tuning of physical and chemical properties. *Science.* 2009; 324:59–63. [PubMed: 19342581]
- [3]. Sands RW, Mooney DJ. Polymers to direct cell fate by controlling the microenvironment. *Curr Opin Biotechnol.* 2007; 18:448–53. [PubMed: 18024105]
- [4]. Zhao F, Yin Y, Lu WW, Leong JC, Zhang W, Zhang J, et al. Preparation and histological evaluation of biomimetic three-dimensional hydroxyapatite/chitosan-gelatin network composite scaffolds. *Biomaterials.* 2002; 23:3227–34. [PubMed: 12102194]
- [5]. Cicha K, Li Z, Stadlmann K, Ovsianikov A, Markut-Kohl R, Liska R, et al. Evaluation of 3D structures fabricated with two-photon-photopolymerization by using FTIR spectroscopy. *J Appl Phys.* 2011; 110:064911-1–064911-5.
- [6]. Kawai K, Suzuki S, Tabata Y, Ikada Y, Nishimura Y. Accelerated tissue regeneration through incorporation of basic fibroblast growth factor-impregnated gelatin microspheres into artificial dermis. *Biomaterials.* 2000; 21:489–99. [PubMed: 10674814]
- [7]. Leclair AM, Ferguson SSG, Lagugné-Labarthe F. Surface patterning using plasma-deposited fluorocarbon thin films for single-cell positioning and neural circuit arrangement. *Biomaterials.* 2011; 32:1351–60. [PubMed: 21074849]
- [8]. Roth EA, Xu T, Das M, Gregory C, Hickman JJ, Boland T. Inkjet printing for high-throughput cell patterning. *Biomaterials.* 2004; 25:3707–15. [PubMed: 15020146]
- [9]. Baran ET, Tuzlakolu K, Salgado A, Reis RL. Microchannel-patterned and heparin micro-contact-printed biodegradable composite membranes for tissue-engineering applications. *J Tissue Eng Regen Med.* 2011; 5:e108–14. [PubMed: 21604378]
- [10]. Doyle AD, Wang FW, Matsumoto K, Yamada KM. One-dimensional topography underlies three-dimensional fibrillar cell migration. *J Cell Biol.* 2009; 184:481–90. [PubMed: 19221195]
- [11]. Wang YC, Ho CC. Micropatterning of proteins and mammalian cells on biomaterials. *FASEB J.* 2004; 18:525–7. [PubMed: 14715699]

- [12]. Mahmud G, Campbell CJ, Bishop KJM, Komarova YA, Chaga O, Soh S, et al. Directing cell motions on micropatterned ratchets. *Nat Phys.* 2009; 5:606–12.
- [13]. Lin X, Helmke BP. Micropatterned structural control suppresses mechanotaxis of endothelial cells. *Biophys J.* 2008; 95:3066–78. [PubMed: 18586851]
- [14]. Lo CM, Wang HB, Dembo M, Yi Wang. Cell movement is guided by the rigidity of the substrate. *Biophys J.* 2000; 79:144–52. [PubMed: 10866943]
- [15]. Rhoads DS, Guan JL. Analysis of directional cell migration on defined FN gradients: role of intracellular signaling molecules. *Exp Cell Res.* 2007; 313:3859–67. [PubMed: 17640633]
- [16]. Kumar G, Co CC, Ho CC. Steering cell migration using microarray amplification of natural directional persistence. *Langmuir.* 2011; 27:3803–7. [PubMed: 21355564]
- [17]. Kumar G, Ho CC, Co CC. Guiding cell migration using one-way micropattern arrays. *Adv Mater.* 2007; 19:1084–90.
- [18]. Kushiro K, Chang S, Asthagiri AR. Reprogramming directional cell motility by tuning micropattern features and cellular signals. *Adv Mater.* 2010; 22:4516–9. [PubMed: 20818616]
- [19]. Kumar G, Wang YC, Co C, Ho CC. Spatially controlled cell engineering on biomaterials using polyelectrolytes. *Langmuir.* 2003; 19:10550–6.
- [20]. Li R, Debreceni B, Jia B, Gao Y, Tigy G, Zheng Y. Localization of the PAK1-, WASP-, and IQGAP1-specifying regions of Cdc42. *J Biol Chem.* 1999; 274:29648–54. [PubMed: 10514434]
- [21]. De Donatis A, Comito G, Buricchi F, Vinci MC, Parenti A, Caselli A, et al. Proliferation versus migration in platelet-derived growth factor signaling. *J Biol Chem.* 2008; 283:19948–56. [PubMed: 18499659]
- [22]. Mader CC, Hinchcliffe EH, Wang Y-l. Probing cell shape regulation with patterned substratum: requirement of myosin II-mediated contractility. *Soft Matter.* 2007; 3:357–63.
- [23]. Ware MF, Wells A, Lauffenburger DA. Epidermal growth factor alters fibroblast migration speed and directional persistence reciprocally and in a matrix-dependent manner. *J Cell Sci.* 1998; 111:2423–32. [PubMed: 9683636]
- [24]. Maheshwari G, Brown G, Lauffenburger DA, Wells A, Griffith LG. Cell adhesion and motility depend on nanoscale RGD clustering. *J Cell Sci.* 2000; 113:1677–86. [PubMed: 10769199]
- [25]. Nobes CD, Hall A. Rho GTPases control polarity, protrusion, and adhesion during cell movement. *J Cell Biol.* 1999; 144:1235–44. [PubMed: 10087266]
- [26]. Pouthas F, Girard P, Lecaudey V, Ly TBN, Gilmour D, Boulin C, et al. In migrating cells, the golgi complex and the position of the centrosome depend on geometrical constraints of the substratum. *J Cell Sci.* 2008; 121:2406–14. [PubMed: 18577576]
- [27]. Pankov R, Endo Y, Even-Ram S, Araki M, Clark K, Cukierman E, et al. A Rac switch regulates random versus directionally persistent cell migration. *J Cell Biol.* 2005; 170:793–802. [PubMed: 16129786]
- [28]. Cory GOC, Ridley AJ. Cell motility: braking WAVES. *Nature.* 2002; 418:732–3. [PubMed: 12181548]



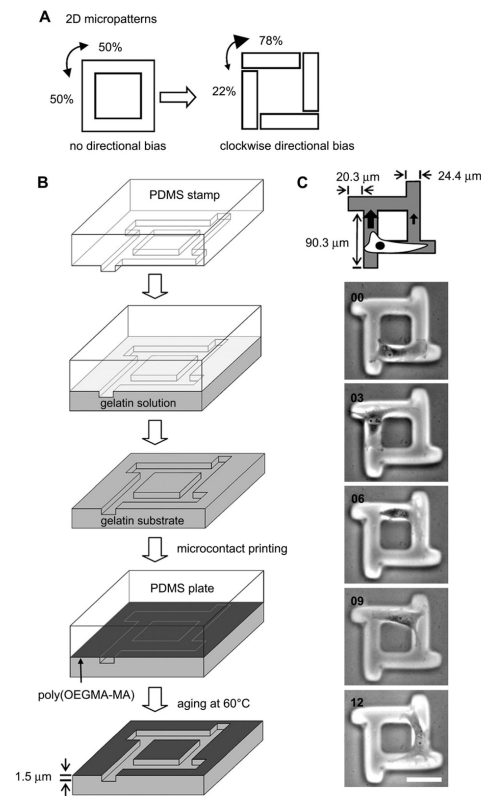


**Fig. 1.** Amplification of natural directional persistence. A) NIH3T3 fibroblasts on continuous two-dimensional adhesive path show no directional bias. When the path is nicked, cells are intermittently confined and the preferential extension of lamellipodia parallel to the extended cell body leads to directional migration in the clockwise direction (Supplementary Fig. 1). B) Schematic procedure for casting gelatin microchannels. C) Cyclic connected rectangular wells with overhangs direct migration of NIH3T3 fibroblast in the preset clockwise direction (time in hours). Scale bar: 50  $\mu\text{m}$ .

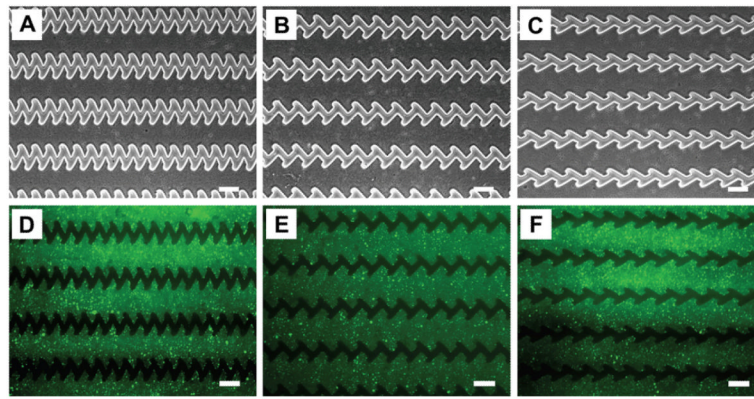


**Fig. 2.** Photomicrographs of overhanging microchannels in gelatin printed with fluorescein-O-methacrylate conjugated poly(OEGMA-MA). Interconnection angles of overhang rectangles are  $60^\circ$  (A),  $90^\circ$  (B) and  $120^\circ$  (C). Fluorescence micrographs (D, E, F) Show selective imprinting of poly(OEGMA-MA) (green) on the plateau regions. Scale bars:  $100\ \mu\text{m}$ . (For interpretation of the references to color in this figure legend, the reader is referred to the web version of this article.)

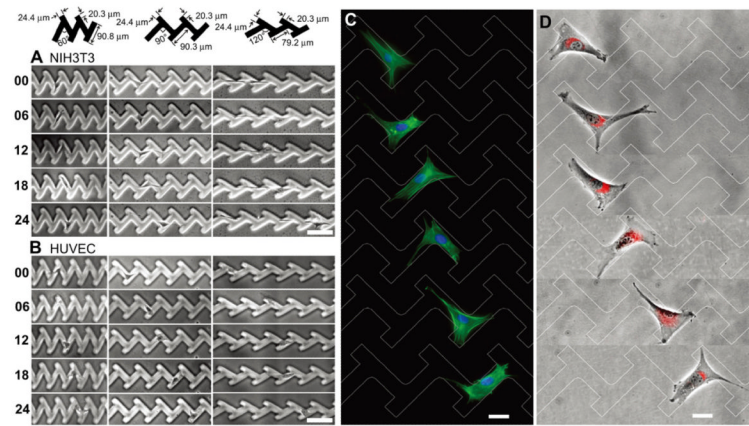


**Fig. 3.** Continuous TANDIP microchannels direct A) NIH3T3 fibroblast and B) human umbilical vein endothelial cells (HUVEC) to preferentially move to the right (time in hours). C & D) Fluorescence images of NIH3T3 fibroblasts on two-dimensional zigzag micropatterns. Cells were stained to observe F-actin (green), nucleus (blue) and Golgi apparatus (red). Scale bars in A, B: 100 μm. Scale bars in C, D: 30 μm.

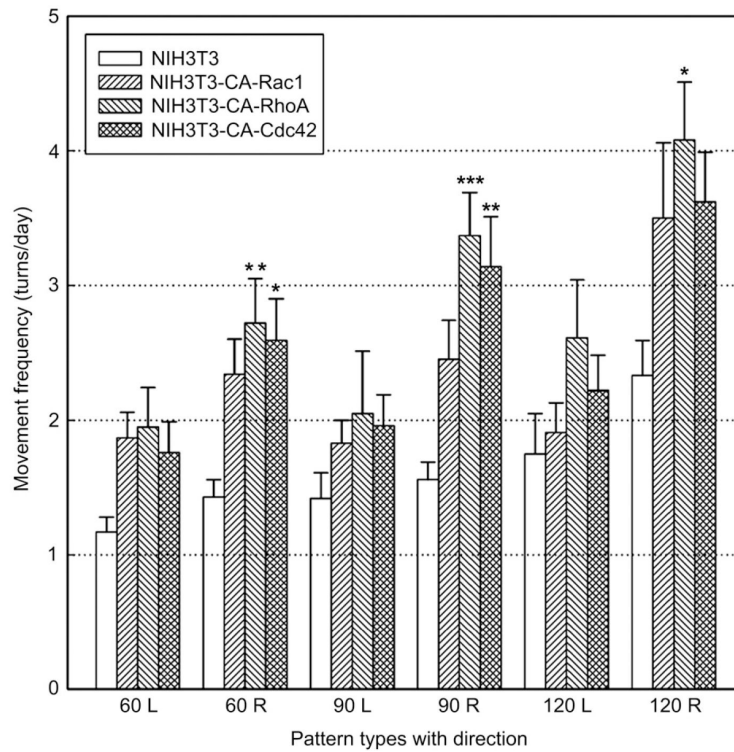


**Fig. 4.** Cell migration frequency towards the left (L) and right (R) for 60°, 90°, and 120° TANDIP microchannels. Data are mean  $\pm$  S.E. for  $n > 50$  cells. \*\*\* $p < 0.001$ , \*\* $p < 0.01$ , \* $p < 0.05$  to NIH3T3 fibroblasts.

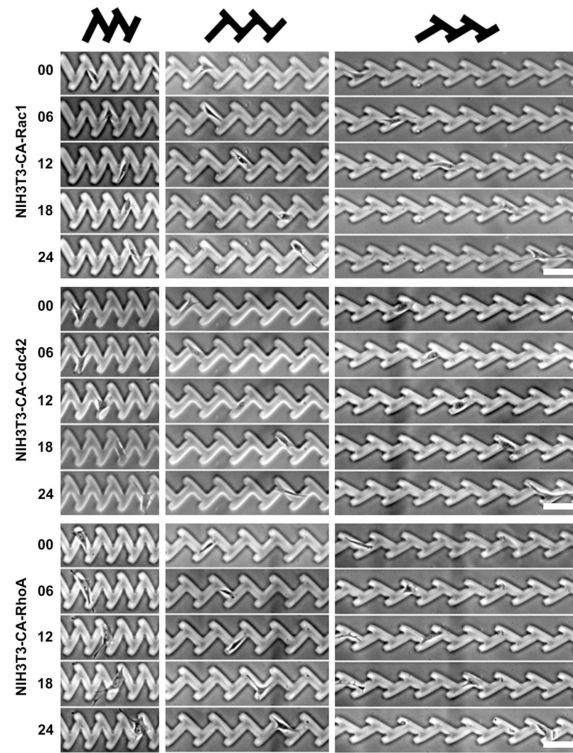


**Fig. 5.** Effects of intracellular signaling and pattern design on directional cell migration. Time-lapse images (in hours) show the movement of NIH3T3 fibroblast mutants with constitutively activated Rac1, Cdc42, and RhoA on 60°, 90° and 120° TANDIP microchannels. NIH3T3-CA-RhoA fibroblasts consistently exhibit the fastest migration speed among NIH3T3 fibroblast mutants. Cell migration speed increases with increasing interconnection angle. Scale bars: 100  $\mu\text{m}$ .

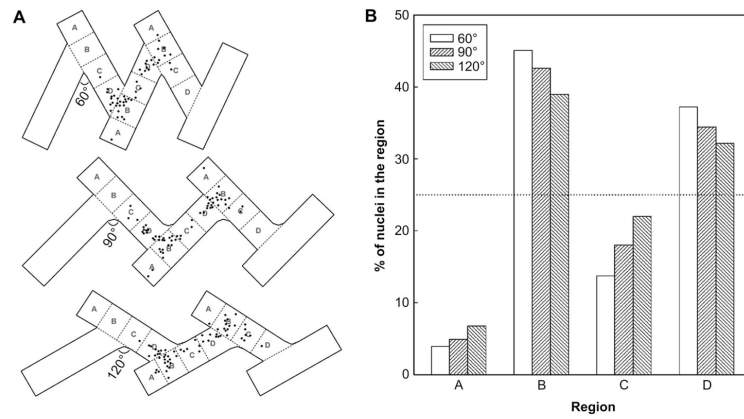




















**Fig. 6.** Cells decelerate as their nuclei pass through the junction turns. A) Nuclei positions were quantified every 6 h from >50 time-lapse micrographs for each pattern design. The dots represent the centroids of nuclei. B) Frequency of the nucleus located in each region (A: overhang, B: T-center, C: middle, D: T-entry).



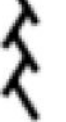


Table 1

Summary of the cell movement on different types of 3D microchannels.

Cell type	Pattern	Number of observed migration [turns]	Bias	Movement frequency [turns/day]	Net horizontal velocity [mm/day]
NIH3T3		 100  28	78%	2.5 ± 1.0	2.2 ± 0.6
NIH3T3		 142  38	79%	3.4 ± 1.8	2.7 ± 1.3
NIH3T3		57	80%	1.4 ± 0.8	1.2 ± 0.4
		61	78%	1.6 ± 0.8	1.4 ± 0.7
		91	76%	2.3 ± 1.6	1.8 ± 1.2
					50
					76
					122

Cell type	Pattern	Number of observed migration [turns]	Bias	Movement frequency [turns/day]	Net horizontal velocity [mm/day]
NIH3T3-CA-Rac1		82	74%	2.3 ± 1.5	1.0 ± 0.7
		93	74%	2.4 ± 1.8	1.8 ± 0.7
		98	70%	3.5 ± 3.0	1.9 ± 1.0
		87	60%	2.7 ± 1.9	2.0 ± 0.3
		101	71%	3.4 ± 2.5	2.0 ± 1.4
		163	78%	4.1 ± 2.7	2.6 ± 1.8
NIH3T3-CA-Cdc42		75	63%	2.6 ± 1.7	1.9 ± 1.2
		88	63%	3.1 ± 2.0	2.0 ± 1.2
		105	64%	3.6 ± 2.0	2.2 ± 1.3

Cell type	Pattern	Number of observed migration [turns]	Bias	Movement frequency [turns/day]	Net horizontal velocity [mm/day]
HUVEC		58	57%	2.0 ± 1.5	1.6 ± 1.0
		73	59%	2.3 ± 1.9	1.9 ± 1.5
		95	74%	3.0 ± 2.8	1.6 ± 1.1